

# Theoretical Studies on the Mechanism, Enantioselectivity, and Axial Ligand Effect of a Ru(salen)-Catalyzed Asymmetric Cyclopropanation Reaction

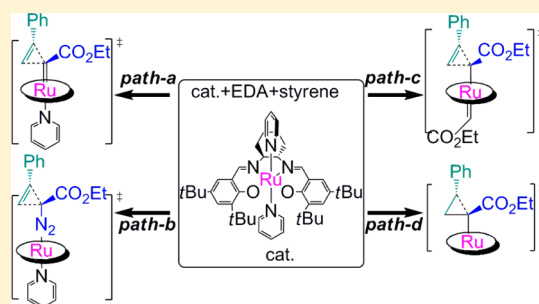
Ting Shi,<sup>†,‡,§</sup> Yu Luo,<sup>‡,§</sup> Xiao-Lei Wang,<sup>†</sup> Shaoyong Lu,<sup>‡</sup> Yi-Lei Zhao,<sup>\*,†</sup> and Jian Zhang<sup>\*,‡</sup>

<sup>†</sup>State Key Laboratory of Microbial Metabolism, School of Life Sciences and Biotechnology, Shanghai Jiao Tong University, 800 Dongchuan Road, Shanghai 200240, People's Republic of China

<sup>‡</sup>Department of Pathophysiology, Key Laboratory of Cell Differentiation and Apoptosis of Chinese Ministry of Education, School of Medicine, Shanghai Jiao Tong University, 280 Chongqing Road, Shanghai 200025, People's Republic of China

## S Supporting Information

**ABSTRACT:** The mechanism of the Ru(salen)-mediated (salen = 1,2-cyclohexanediamino-*N,N'*-bis(3,5-di-*tert*-butylsalicylidene)) cyclopropanation reaction of styrene with ethyl diazoacetate (EDA) is explored with density functional theory (DFT) methods. Five proposed reaction pathways, including (1) a stepwise process containing the formation of carbene species and cyclopropanation step (path a), (2) a one-step process (path b), (3) a bis-carbene mechanism (path c), (4) a three-centered-intermediate pathway (path d), and (5) the main side reaction of dimerization of EDA (path e), are taken into consideration to determine the most favorable mechanism. Computational results indicate that path a with a barrier of 27.9 kcal/mol (*trans*) is superior to all other pathways. The geometries of the critical transition states are picked out for further analyses. It is found that the C–H<sup>a</sup> group of the catalyst plays a key role in enantioselectivity. The destruction of the active center (for example, a methyl group substituent) can dramatically decrease the catalytic efficiency. In addition, the axial ligands are found to mediate energy barriers of the formation of carbene species and the cyclopropanation step in entirely opposite directions. The natural bond orbital (NBO) analyses demonstrate that carbene species show different characteristics of Fischer- or/and Schrock-type complexes. This study may help to design and develop more efficient catalysts for metal-mediated cyclopropanation reactions.



## INTRODUCTION

Compounds containing the cyclopropane fragment have received considerable attention because of their frequent occurrence in natural products and bioactive compounds.<sup>1</sup> Cyclopropanes are also found to undergo a wide array of synthetically useful transformations as versatile building blocks in organic synthesis.<sup>2</sup> One of the most common methods for synthesizing cyclopropanes is transition-metal-catalyzed cyclization of diazo esters with olefins.<sup>3</sup> Since the seminal introduction of metal-mediated asymmetric cyclopropanation by Nozaki et al.,<sup>4</sup> significant efforts have been devoted to the development of transition-metal-catalyzed enantioselective cyclopropanation reactions. For examples, the Ru(II)–2,6-bis(2-oxazolin-2-yl)pyridine (pybox),<sup>5</sup> Co(II)–porphyrin,<sup>6</sup> and Ru–porphyrin complexes<sup>7</sup> are some of the most efficient catalysts. Among a number of highly active and robust catalysts, metal salen complexes with four coordinating sites (O, N, N, and O) and two axial sites open to ancillary ligands are particularly versatile for the design of both *cis/trans* and intramolecular/intermolecular cyclopropanation reactions.<sup>8</sup> In addition to their successful catalytic applications in cyclopropanation, metal salen complexes have also been found to be efficient catalysts in various organic transformations such as asymmetric

epoxidation,<sup>9</sup> aziridination,<sup>10</sup> sulfimidation,<sup>11</sup> Diels–Alder reactions,<sup>12</sup> and C–H amination.<sup>13</sup>

Despite the remarkable experimental achievements of metal salen catalysts in cyclopropanation reactions, theoretical studies on these systems are quite rare. Recently, Takatani et al.<sup>14</sup> obtained the electronic structures of d<sup>4</sup> (d<sup>6</sup>) metal–salens with DFT methods,<sup>15</sup> but no reaction pathway was discussed. In 2009, asymmetric intramolecular alkene cyclopropanation was investigated by Xu et al., where a nonplanar salen configuration shows a better catalytic activity than the planar salen complex.<sup>8c</sup> In addition, Yamada and co-workers studied the reaction mechanisms of the cobalt(II)–salen complex catalyzed cyclopropanation reaction with DFT methods. However, these studies were restricted to information about simplified models with small substrates (e.g., ethene and diazoacetaldehyde).<sup>16</sup> In 2002, a series of chiral ruthenium salen catalysts employed by Nguyen et al. in asymmetric intermolecular cyclopropanation of styrene with EDA were reported. They turn out to be very efficient catalysts with exceptionally high enantioselectivity (up to 98% ee; Figure 1).<sup>17</sup>

Received: September 26, 2013

Published: July 10, 2014

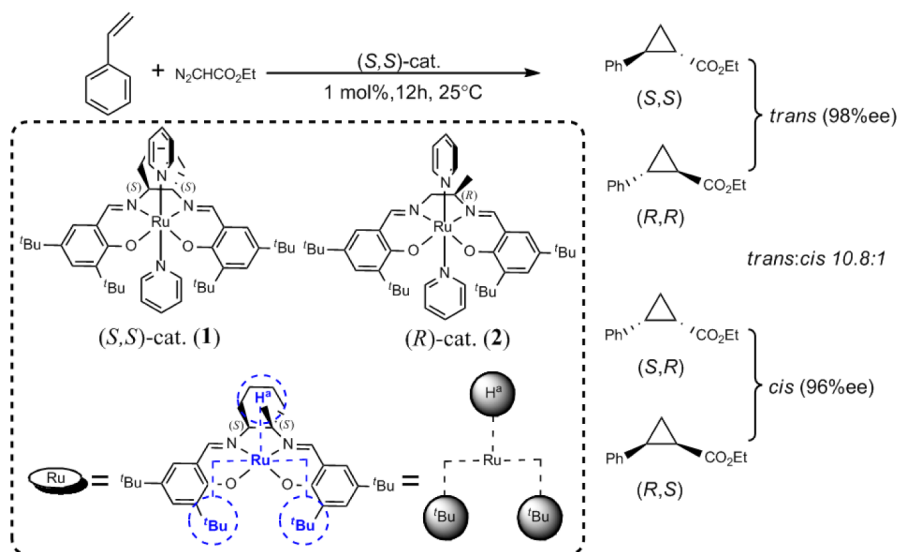


Figure 1. Ru(salen)-catalyzed cyclopropanation reaction reported by Nguyen et al.<sup>17</sup>

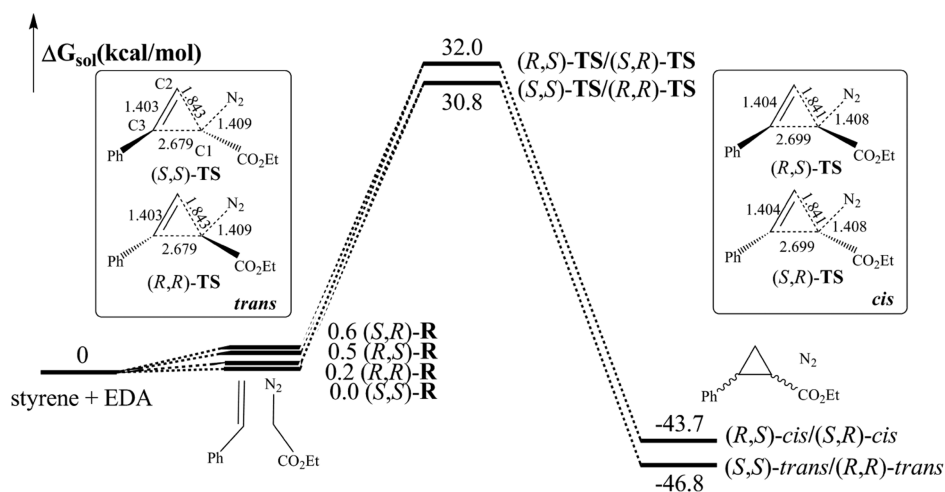


Figure 2. Free energy profile for the uncatalyzed cyclopropanation of styrene with EDA. R stands for the initial complex formation.

To our knowledge, no theoretical study of these Ru(salen)-catalyzed cyclopropanation reactions has ever been reported. Thus, we conducted a computational study with DFT methods to investigate the reaction mechanism of the cyclopropanation and the essence of the high enantioselectivity of the catalyst. Several reaction pathways, including catalyzed and uncatalyzed cyclopropanation reactions, catalytic processes via different intermediates, and the side reaction of EDA dimerization, are proposed in this work. The origin of the high enantioselectivity is rationalized through analyzing the critical structures of transition states. Furthermore, the influence of different axial ligands on the Ru(salen)-catalyzed asymmetric cyclopropanation reaction is studied. Finally, a natural bond orbital (NBO)<sup>18</sup> analysis has been performed to investigate the ligand effect of this reaction. This work aims to shed light on the underlying catalytic mechanism of the reaction, including the nature of the active intermediates and the origin of the high enantioselectivity in the transition states contributing to expand the substrate scope and rationally design more active, selective, and robust catalysts.

## METHODS

To fully understand the reaction mechanism of the Ru-catalyzed cyclopropanation of styrene with EDA, we employ DFT methods to investigate the electronic structure and energetics along the reaction potential energy surface (PES), where the effect of solvent is considered with the polarizable continuum medium (PCM)<sup>19</sup> model. All calculations have been performed with Gaussian 09 software package.<sup>20</sup>

The geometries discussed in this work are fully optimized in the gas phase at the B3LYP<sup>21</sup>/6-31G\*<sup>22</sup> or B3LYP/[6-31G\*, Lanl2dz<sup>23</sup>] level, where the basis set 6-31G\* is employed for H, C, N, and O atoms and Lanl2dz for Ru when it is involved. Frequency calculations have been carried out to confirm the nature of the stationary points. The zero-point energies and the thermal correction at 298.15 K and 1 atm are obtained with the harmonic approximation at optimized structures. The larger basis sets 6-311+G\*\*<sup>24</sup> for H, C, N, and O atoms are utilized to further refine the relative energies by single-point calculations. The PCM model, SMD,<sup>25</sup> is also employed to evaluate the influence of solvent on the PES with single-point calculations at a high level. Solvent effects are taken into account in relative energies discussed in this work without exception.

It should be noted that different density functionals may vary from each other in predicting reaction barriers. Our evaluation of three typical density functionals (B3LYP, M06,<sup>26</sup> PBE1PBE<sup>27</sup>) in gas and

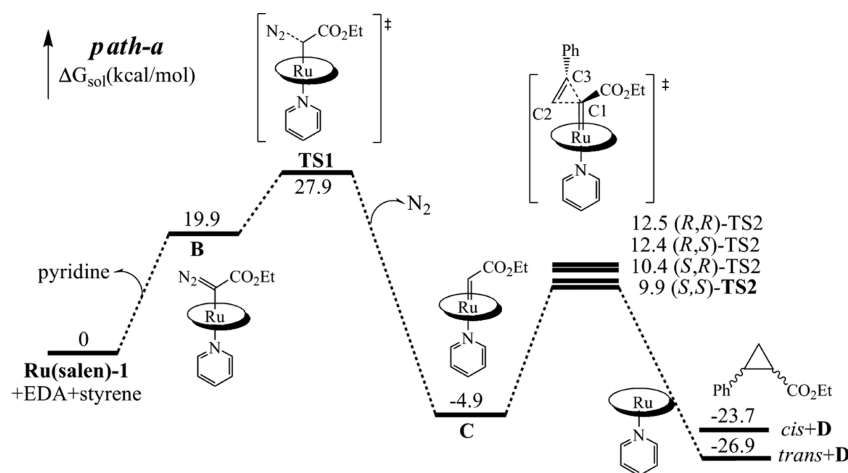


Figure 3. Reaction pathway of Ru(salen)-1-catalyzed cyclopropanation reaction through a stepwise process (path a).

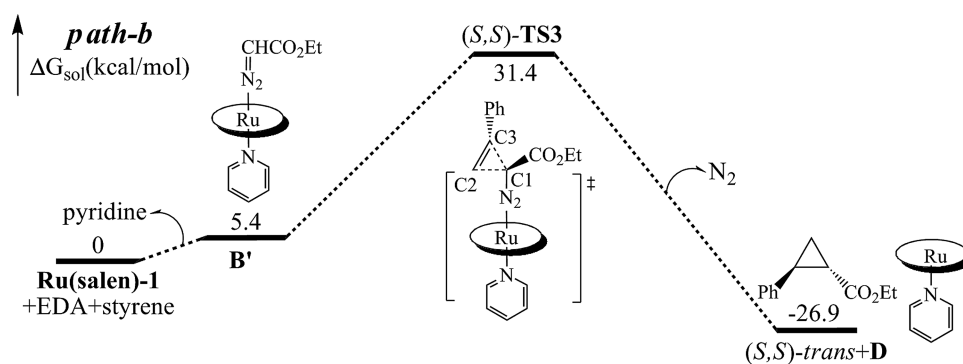


Figure 4. Reaction pathway of the Ru(salen)-1-catalyzed cyclopropanation reaction via a single reaction step (path b).

solvent phases shows that they predicted similar results and led to the same discussion and conclusions for the studied ruthenium systems (see Table S1, Supporting Information). Herein we choose the widely used B3LYP method for our study.

NBO analysis has been carried out on some key structures in order to investigate the stabilizing donor–acceptor interactions and the nature of the Ru–C bonds in ruthenium carbene intermediates. The natural population type (NPT) charges<sup>18c</sup> obtained by natural population analysis (NPA) on metal and carbene carbon, the bond lengths between the metal center and carbene carbon center, and their Wiberg bond indexes are collected for carbene species C, F, and I.

## RESULTS AND DISCUSSION

**1. Uncatalyzed Cyclopropanation Reaction.** The cyclopropanation between EDA and styrene is a single concerted step, in which the cyclopropanation cooperates with the elimination of N<sub>2</sub> molecule from EDA, leading to the formation of ethyl 2-phenylcyclopropanecarboxylate product. The reaction in the absence of catalyst proceeds through nucleophilic attack from the C2 atom of styrene on C1 attached to dinitrogen of EDA (Figure 2). When the approaching and reception directions are considered, four isomers will be obtained, including (*S,S*)-*trans*, (*R,R*)-*trans*, (*R,S*)-*cis*, and (*S,R*)-*cis*. The four calculated reaction pathways with optimized structures of transition states are shown in Figure 1. The reactive center shows no obvious difference between two *trans* isomer transition states either in energy barrier or in geometry, since they are racemates, and this is also valid for the *cis* isomers. The free energy barriers are 32.0 and 30.8 kcal/mol for the *trans* and *cis* pathways, respectively. Obviously, the *trans*

pathway is favored by 1.2 kcal/mol in comparison with the *cis* pathway, which will dominate the high *trans* selectivity.

**2. Ru(salen)-1-Catalyzed Cyclopropanation Reaction.**  
**2.1. Catalytic Reaction Pathway with a Stepwise Process (Path a).** Different from the uncatalyzed cyclopropanation, most existing transition-metal-catalyzed cyclopropanation systems share a general mechanism,<sup>6g,16a</sup> in which the catalysts react with the diazo compound to produce metal carbenes that are subsequently attacked by the alkenes to provide the cyclopropanes and regenerate the catalysts. Herein, we proposed a catalytic pathway (path a) with such a stepwise process for the Ru(salen)-1-catalyzed cyclopropanation reaction (Figure 3).

Path a begins with the replacement of an axial pyridine ligand of Ru(salen)-1 by EDA to the methine C-bound complex B, where the C1 atom of EDA is coordinated to the ruthenium atom of the catalyst. The ruthenium carbene species C is generated after releasing a N<sub>2</sub> molecule via transition state TS1. The chiral carbon atom C2 of styrene reacts with the carbene by approaching from the *Re* or *Si* face to provide *trans/cis* cyclopropane products and the active catalyst D. In the next cycle, D would bind to another EDA to form carbene species C. Our computational results demonstrated that, in path a, the formation of the ruthenium carbene species C is the rate-determining step with a free energy of 27.9 kcal/mol, and the energy barrier of the next cyclopropanation step to the (*S,S*)-*trans* product is 14.8 kcal/mol.

**2.2. Catalytic Reaction Pathway with a Single Step (Path b).** In addition to the carbon-bound adduct B, the DFT

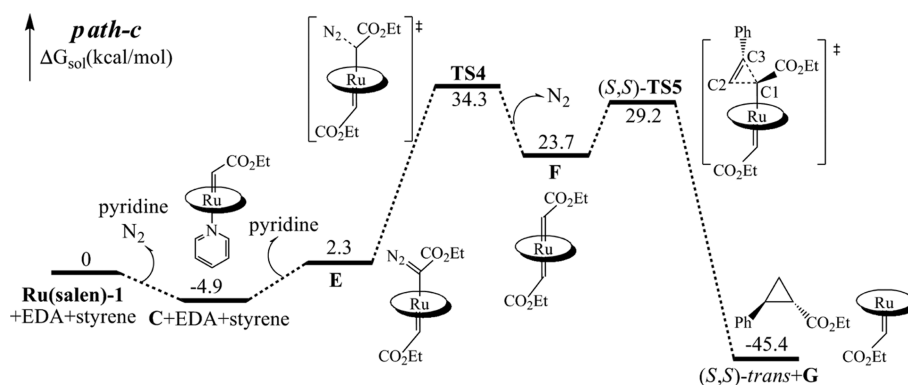


Figure 5. Reaction pathway of the Ru(salen)-1-catalyzed cyclopropanation reaction via the bis-carbene intermediate F (path c).

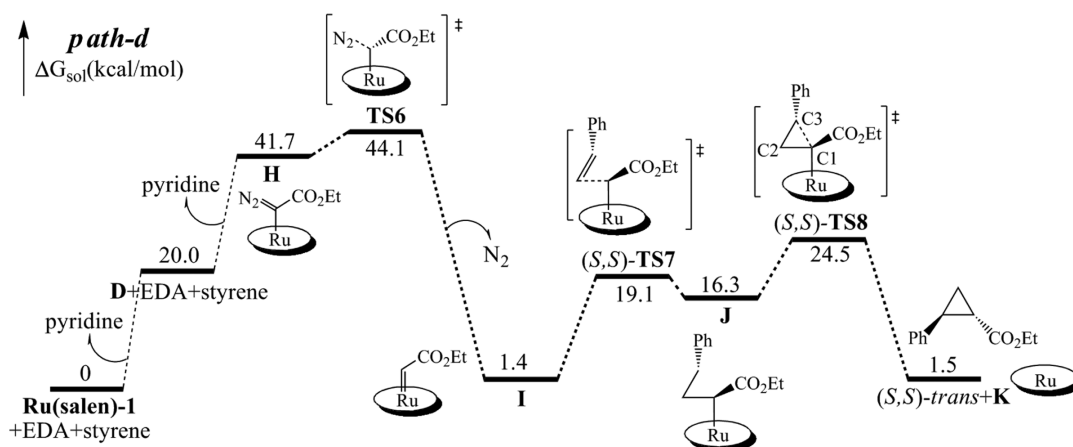


Figure 6. Reaction pathway of the Ru(salen)-1-catalyzed cyclopropanation reaction via the three-centered intermediate J (path d).

calculations predict the availability of nitrogen-bound complex B', which is 14.5 kcal/mol lower than B in energy, is +5.4 kcal/mol uphill relative to the reagent triad (catalyst, EDA, and styrene). Therefore, path b is proposed to investigate the reactive possibility starting with B'. The reaction reveals a one-step process via TS3 to obtain cyclopropane products and the active catalyst D: that is, the elimination of the N<sub>2</sub> molecule synchronizes with the formation of the cyclopropane products and no ruthenium carbene species is involved. Only the pathway to forming the dominant (*S,S*)-*trans* isomer is shown in Figure 4. The energy barrier of path b is 31.4 kcal/mol, which is 3.5 kcal/mol higher than that of path a. Thus, the catalytic reaction pathway with a single step should be neglected, and more attention should be paid to path a via a metal carbene intermediate.

**2.3. Catalytic Reaction Pathway with the Ru(salen) Bis-Carbene Intermediate F (Path c).** A mechanistic study on Os(TTP)-mediated (TTP = 5,10,15,20-tetra-*p*-tolylprophyrinato) cyclopropanation<sup>28</sup> indicated that the osmium bis-carbene species is the active catalyst. Does it also apply to the Ru(salen) system? How does the bis-carbene intermediate influence the energy barrier of the cyclopropanation reaction? Here we address these questions on path c with a Ru(salen) bis-carbene intermediate.

The reaction starts with the carbene intermediate C, which accepts an EDA molecule to form the methine C-bound complex E, and then E releases a N<sub>2</sub> molecule via TS4 to give the bis-carbene species F. The bis-carbene F reacts with styrene to complete the cyclopropanation reaction, and the cyclo-

propane products and the single carbene species G were finally produced. The calculated free energies for Ru(salen)-1-catalyzed cyclopropanation to the dominant (*S,S*)-*trans* cyclopropane product are plotted in Figure 5. In the process, the formation of the Ru(salen) bis-carbene F is identified as the rate-determining step with a free energy barrier of 39.2 kcal/mol. Therefore, the bis-carbene mechanism is difficult for the Ru(salen)-catalyzed system. Interestingly, it should be noted that the energy barrier of the cyclopropanation step significantly decreases to 5.5 kcal/mol in comparison with that in path a (14.8 kcal/mol), suggesting that the carbene ligand will remarkably facilitate the cyclopropanation step.

**2.4. Catalytic Reaction Pathway with the Three-Centered Intermediate J (Path d).** To fully investigate the effect of the axial ligand, the cyclopropanation reaction mediated by a vacant axial ligand is also studied. The reaction pathway (Figure 6) is proposed to start with the single-pyridine-coordinated intermediate D. Then the pyridine of D is replaced by EDA to give the methine C-bound complex H, which eliminates a N<sub>2</sub> molecule via TS6 to generate the single carbene species I. The addition of carbene species to the styrene proceeds via TS7 and eventually the ring-closing step via TS8 to afford cyclopropane enantiomers and ruthenium salen catalyst K without any axial ligand. Different from the pathways mentioned above, the cyclopropanation reaction affords a three-centered or four-centered intermediate. In the three-centered pathway (path d), the terminal carbon atom (C2) of styrene directly attacks at the carbene carbon atom C1 to form the CHCO<sub>2</sub>EtCH<sub>2</sub>CHPh intermediate J, whereas in the four-

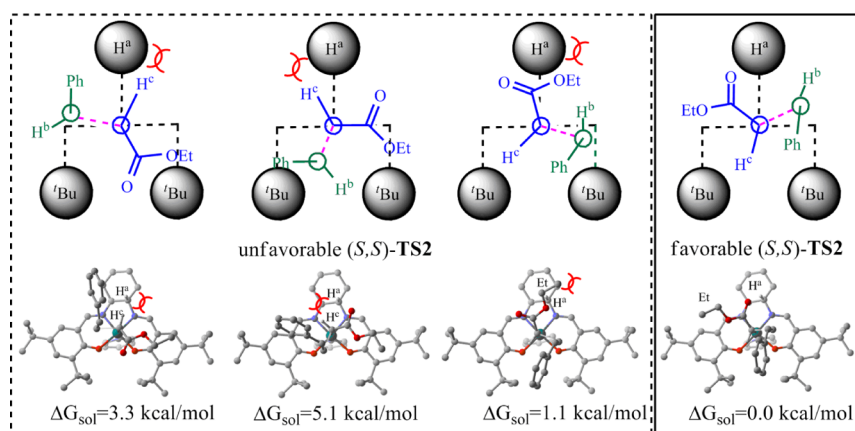


Figure 7. Selected transition states of (*S,S*)-TS2 with different steric hindrance.

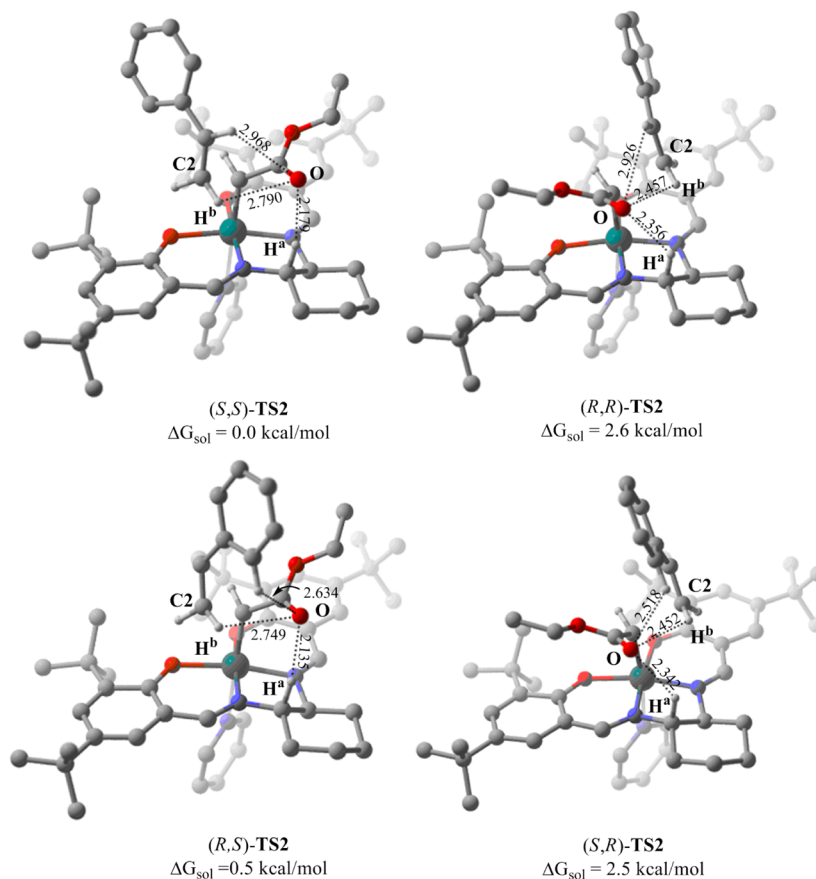
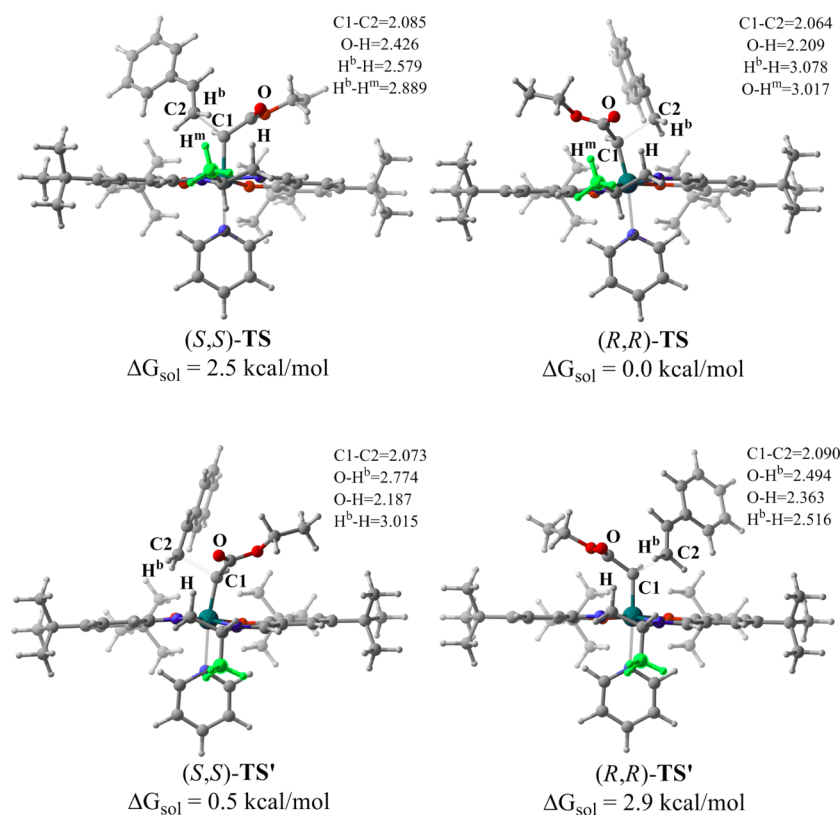


Figure 8. Optimized transition states of TS2 with key parameters. Free energies with PCM from the B3LYP[6-311+G\*\*, Lan12dz]//B3LYP/[6-31G\*, Lan12dz] method are shown.

centered pathway, the metallacyclobutane intermediate **J'** is formed (path d' in Figure S1 (Supporting Information)). Our computational results indicate that the energy barrier of the carbene formation step remarkably decreases to 2.4 kcal/mol in comparison with that in path a (8.0 kcal/mol) and the barrier of the cyclopropanation step increases to 23.1 kcal/mol in comparison with that in path a (14.8 kcal/mol), suggesting the vacant axial ligand might have a different influence in the formation of carbene species and the cyclopropanation step.

As reported by Yamada,<sup>16a</sup> there could be no intermediates in the ring-closure step, suggesting that the potential energy surface might be very flat. In addition, the ring-closure reactions

reported by Bruin<sup>6g</sup> with generation of the “ $\gamma$ -alkyl radical” type species  $\text{Co}(\text{por})(\text{CHCO}_2\text{MeCH}_2\text{CHR}^*)$  ( $\text{R} = \text{CH}_3, \text{Ph}, \text{CO}_2\text{Me}$ ) are processes with very low barriers (<2.6 kcal/mol). According to our calculations, the energy barrier of the ring-closure step in path d is calculated to be 8.2 kcal/mol. In comparison with the  $\gamma$ -alkyl radical species, our intermediate **J**,  $[\text{Ru}(\text{salen})(\text{CHCO}_2\text{EtCH}_2\text{CHPh})]$ , is a more stable complex, and we think this can be attributed to the slight increase of the energy barrier. Furthermore, it has also been pointed out by Fischer<sup>29</sup> that the barrier for cyclopropane ring closure would have to be higher than 8 kcal/mol to counteract the activation energy for addition of olefinic monomers to a growing radical



**Figure 9.** Optimized transition states TS and TS' with key parameters. The functional methyl groups occupying the axial and equatorial positions are depicted in green.

polymer chain. Our computational results are in accord with these conclusions.

We have also tried to find an analogous three-centered intermediate and its transition states in path a. However, despite several attempts to optimize the intermediate and approach the problem with different constraint geometry variations, we were unable to find such geometries.

**3. Enantioselectivity of the Ru(salen)-Catalyzed Cyclopropanation Reaction.** **3.1. Selectivity of the Cyclopropanation Reaction Catalyzed by Ru(salen)-1.** The optimized geometries of (S,S)-TS2 have been carefully investigated to study the stability of possible transition states. Four transition states leading to the (S,S)-*trans* enantiomers are obtained, and their geometries are demonstrated in Figure 7. In detail, the hydrogen (designated as H<sup>c</sup>) attached to C1 of carbene species C can adopt, in principle, two different orientations when styrene attacks. One is pointing at the steric hydrogen (H<sup>a</sup>) of the chiral carbon of cyclohexane; the other is opposite from H<sup>a</sup>. Our computational results suggest that transition states with the former conformation are higher in energy than the latter transition states. The steric interaction between the C–H<sup>a</sup> group and the C–H<sup>c</sup> group is mostly responsible for the energy difference. On the other hand, the ester group of C also can adopt two different conformations to influence the energy of the transition state. As demonstrated in Figure 7, the proper orientation of the ester group will help to stabilize the transition state. These conformational analyses demonstrated that steric interactions play a critical role in determining the final enantioselectivity of the cyclopropane enantiomers.

Furthermore, four transition states (including (S,S)-TS2/(R,R)-TS2 and (R,S)-TS2/(S,R)-TS2) have been carefully

analyzed to shed light on the origin of the high enantioselectivity. A prominent interaction is found between the carbonyl oxygen (O) of acetate and the hydrogen (H<sup>a</sup>) attached to the chiral carbon of cyclohexane. According to our calculations the charge of H<sup>a</sup> ( $\sim 0.20e$ ) is more positive than that of the other hydrogens ( $\sim 0.14e$ ) in cyclohexane, which will facilitate the O $\cdots$ H<sup>a</sup> H-bond formation between the carbonyl oxygen of acetate and H<sup>a</sup>. As expected, (S,S)-TS2 and (R,S)-TS2 have more matched electronic orientations between H<sup>a</sup> and the lone pair of the oxygen of acetate in comparison to (R,R)-TS2 and (S,R)-TS2, since the O–H<sup>a</sup> distances are 2.135, 2.179, 2.342, and 2.356 Å in (R,S)-TS2, (S,S)-TS2, (S,R)-TS2, and (R,R)-TS2, respectively. This order is almost reflected in the energetic sequence. Actually, (S,S)-TS2 and (R,S)-TS2 are found to be much lower in free energy than (R,R)-TS2 and (S,R)-TS2. On the other hand, (S,S)-TS2 is found to be more stable than (R,S)-TS2. The repulsion between the acetate group and the benzene ring of styrene is proposed to be responsible for the energy gap. In detail, the *trans* transition state of (S,S)-TS2 is 0.5 kcal/mol lower in free energy than the *cis* transition state of (R,S)-TS2. Optimized structures of TS2 with key parameters and free energies are demonstrated in Figure 8.

Since the cyclopropanation reactions are subject to the Curtin–Hammett principle, the (S,S)-*trans*/(R,R)-*trans* product ratio can be estimated, and the calculated ee value is 99.4%. Fortunately, this result is in excellent agreement with the experimental value of 98% ee described by Nguyen.<sup>17</sup> In addition, according to Nguyen's experiments (*trans*/*cis* = 10.8/1), the energy difference between (S,S)-TS2 and (R,S)-TS2 is  $\sim 1.4$  kcal/mol. Our computational result is 0.5 kcal/mol, which is roughly consistent with the experiment.

**3.2. Selectivity of Cyclopropanation Reaction Catalyzed by Ru(salen)-2.** To get a deep insight into the diastereo- and enantioselectivity of the catalyzed cyclopropanation reaction, the reaction mechanism catalyzed by Ru(salen)-2 (Figure 1), another efficient ruthenium catalyst reported by Nguyen, has also been investigated with the same methods mentioned above. The main difference between them lies near the chiral center, where the cyclohexane of Ru(salen)-1 is replaced by a methyl group of Ru(salen)-2. It is known that the methyl group could occupy axial and equatorial positions to avoid unfavorable interactions; thus, transition states with both CH<sub>3</sub>-axial and CH<sub>3</sub>-equatorial conformers are obtained and relative stable structures are shown in Figure 9.

It can be seen that the CH<sub>3</sub>-equatorial transition state (*S,S*)-TS is structurally less favorable than the alternative CH<sub>3</sub>-equatorial (*R,R*)-TS, due to steric hindrance between the C–H<sup>m</sup> group (hydrogen of the methyl group) and the C–H<sup>b</sup> group; thus, the CH<sub>3</sub>-equatorial (*R,R*)-TS is found to be 2.5 kcal/mol more stable than the CH<sub>3</sub>-equatorial (*S,S*)-TS. In addition, the computational results reveal that the energy of the CH<sub>3</sub>-axial (*R,R*)-TS' structure is 2.4 kcal/mol lower than that of the CH<sub>3</sub>-axial (*S,S*)-TS' in solvent. Apparently, the results indicate that the reaction to produce (*R,R*)-*trans* via the CH<sub>3</sub>-equatorial (*R,R*)-TS is the most favorable process among these four pathways when both thermodynamic and kinetic factors are considered. Also, as the cyclopropanation reactions are subject to the Curtin–Hammett principle, the (*R,R*)-*trans*/*S,S*)-*trans* product ratio based on (*R,R*)-TS/(*S,S*)-TS' ( $\Delta\Delta G_{\text{sol}} = 0.5$  kcal/mol) can be estimated, and the calculated ee value is 39.8%, which is near the experimental value of 12% ee.

**4. Axial Ligand Effects.** So far the focus has been on exploring possibilities of the cyclopropanation of styrene with EDA catalyzed by Ru(salen). To study the influence of different axial ligands on the reaction, the energy barriers for the formation of carbene species and the cyclopropanation step in paths a, c, and d were picked out for deep analyses (Figure 10).

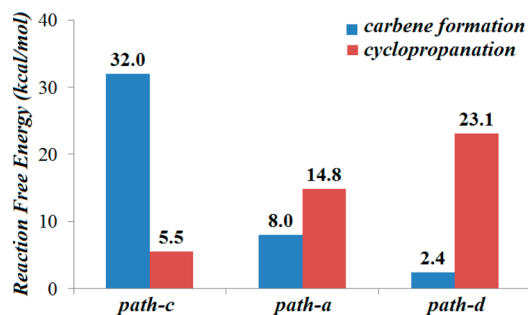


**Figure 10.** Free energies of carbene formation and cyclopropanation steps in paths a, c, and d.

The axial ligands are pyridine, carbene, and none in paths a, c, and d, respectively. It is noteworthy that the carbene ligand dramatically reduces the activation energy for the cyclopropanation step, but at the same time it increases the energy barrier of carbene formation. This is not so with the vacant axial ligand, which clearly reduces the activation energy of carbene formation and enhances the energy barrier of the cyclopropanation step. Our calculations reveal that the axial donor ligand produces two prominent effects. One is to reduce the activation energy for the formation of the ruthenium carbene complex, while the other is to increase the energy barrier of the cyclopropanation step. Figure 10 summarizes the activation

energies of each step for the respective axial ligand. It can be seen that the activation energy for the formation of F, C, and I decreases from 32.0 (path c) to 8.0 (path a) to 2.4 kcal/mol (path d). On the other hand, the energy barrier of the cyclopropanation step increases from 5.5 (path c) to 14.8 (path a) to 23.1 kcal/mol (path d).

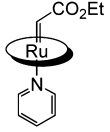
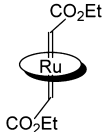
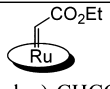
Natural bond orbital (NBO) analyses have been carried out to investigate the different ligand effects and associated electronic properties on carbene species C, F, and I. Three parameters of the optimized electronic structures have been collected for the three carbene species: that is, the natural population type (NPT) charges on the metal center and carbene carbon center, the bond lengths between the metal center and carbene carbon center, and their Wiberg bond indexes (Table 1). As the standard Fischer<sup>30</sup> and Schrock-type<sup>31</sup> carbene complexes, tungsten and titanium carbene species are also gathered in Table 1 for comparisons.

Carbene species F has a weaker metal carbene bond index of 1.182 (1.98 Å) and less negative partial charge on the carbene carbon (−0.106e), which resembles the nature of a Fischer-type complex. Carbene species I has a stronger metal carbene bond index of 1.590 (1.84 Å) and more s negative partial charge on the carbene carbon (−0.187e), similar to the case for Schrock-type carbene complexes. This is validated by the NBO analyses, which show that  $\sigma$  donation occurs between the sp<sup>2</sup> orbital of the carbene carbon and the singly occupied d<sub>z<sup>2</sup></sub> orbital of the ruthenium atom and back-donation from the  $\pi$  orbitals of the ruthenium into the  $\pi^*$  of the ruthenium–carbene bond (see the Supporting Information, Figure S2). Furthermore, ruthenium carbene C has the characteristic of activating the nucleophile showing a Schrock-type nature, since the metal carbene bond index and the bond distance are near to those of the Schrock type (1.535 and 1.86 Å).

**5. Formation of Side Products DEF and DEM.** Dimerization of diazo compounds to fumarates and maleates is the main side reaction in cyclopropanation mediated by most transition-metal catalysts. In the case of the ruthenium systems, one of the advantages of using Ru(salen) catalysts for cyclopropanation is their significantly suppressed carbene dimerization activity under practical catalytic conditions. The experimental results indicated that the presence of the dimeric side products diethyl fumarate (DEF) and diethyl maleate (DEM) is less than 1%.

To get some insight into the reasons behind the low dimerization activity, the formations of DEF and DEM are expanded to our calculations (Figure 11). The calculated pathway for dimerization reveals the two similar transition states TS9 and TS9' for DEF and TS10 and TS10' for DEM. The main difference between them is the orientation of the dinitrogen group. These reactions are followed by loss of dinitrogen from the diazo compound with simultaneous formation of DEF and DEM in both cases. Apparently formation of the thermodynamically favored DEF is kinetically suppressed (24.7 and 24.4 kcal/mol for TS9 and TS9', respectively). The steric influence between the attacking EDA and substituents at the 5,5'-positions of the salen ligand might be responsible for the high energy barrier. Since the calculated energy barrier for dimer formation is slightly higher than the barriers for cyclopropanation (path a), carbene dimerization is expected to be suppressed, which is in agreement with experimental observations under the catalytic conditions.

Table 1. NPT Charges, Bond Lengths, and Wiberg Bond Indexes<sup>a</sup>

Label	complex	Q <sub>M</sub>	Q <sub>C</sub>	r(M-C)	WBI <sub>M-C</sub>
Fischer-type (FC) <sup>29</sup>	(CO) <sub>5</sub> W-C(CH <sub>3</sub> )OCH <sub>3</sub>	-1.91	0.701	2.01	0.702
Schrock-type (SC) <sup>30</sup>	(C <sub>3</sub> H <sub>5</sub> ) <sub>2</sub> Ti-CH <sub>2</sub>	0.655	-0.860	1.93	1.58
<b>C</b>	 Py-Ru(salen)-CHCO <sub>2</sub> Et	0.307	-0.140	1.86	1.535
<b>F</b>	 EtO <sub>2</sub> CCH-Ru(salen)-CHCO <sub>2</sub> Et	0.090	-0.106	1.98	1.182
<b>I</b>	 Ru(salen)-CHCO <sub>2</sub> Et	0.408	-0.187	1.84	1.590

<sup>a</sup>Bond lengths  $r(M-C)$  are given in Å, charges  $Q$  are given in e, and Wiberg bond indexes  $WBI_{M-C}$  are unitless. M refers to the metal, and C refers to the carbene carbon.

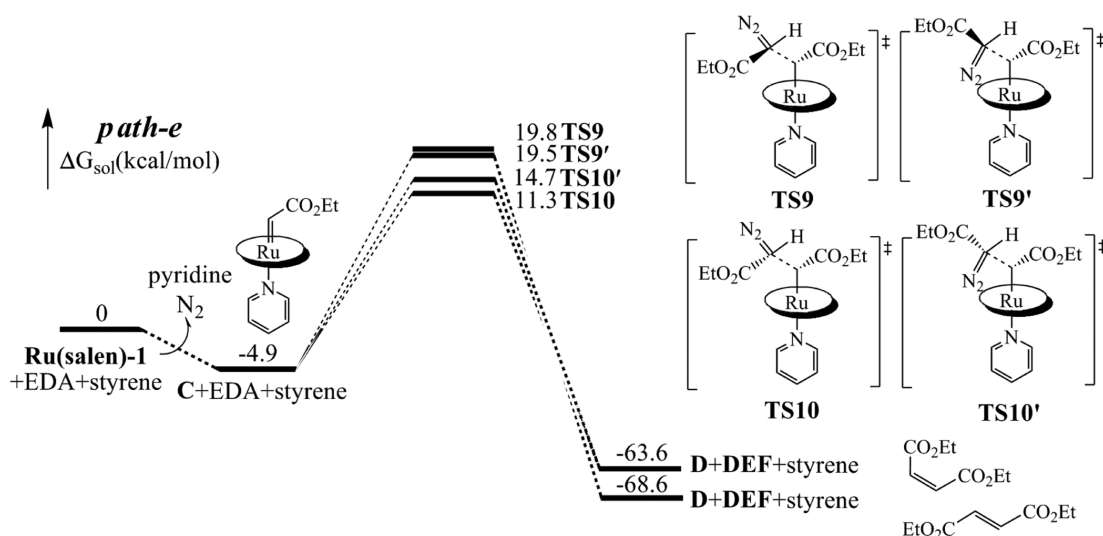


Figure 11. Formation of DEF and DEM by dimerization of EDA.

## CONCLUSION

The mechanism of the Ru(salen)-catalyzed cyclopropanation reaction of styrene with EDA has been extensively investigated by DFT (B3LYP[6-311+G\*\*, Lanl2dz]/B3LYP/[6-31G\*, Lanl2dz]) methods. Our computational study reveals that this cyclopropanation reaction proceeds through a stepwise process including the formation of carbene species and a ring closure step to provide the cyclopropane enantiomers and regenerate the catalyst. The free energy of path a is calculated to be 27.9 kcal/mol. Furthermore, exhaustive mechanistic investigations have been presented: (1) path b goes through a one-step process, (2) path c proceeds through a bis-carbene mechanism, (3) a three-centered-intermediate pathway (path d) is compared to a four-centered-intermediate pathway (path d'), and (4) a main side reaction of dimerization of EDA (path e) is investigated. The geometries of transition states are carefully studied. It is found that the C-H<sup>δ</sup> group of the catalyst plays a

key role in determining the enantioselectivity. The methyl group substituent in Ru(salen)-2 dramatically decreases the catalytic efficiency. Moreover, the axial ligand effect demonstrates that the ligand mediates the energy barriers for the formation of carbene species and the cyclopropanation step in entirely opposite directions: that is, when a ligand favors the formation of carbene species, it will disfavor the cyclopropanation step at the same time. The characters of carbene complexes have been analyzed by NBO methods. Our calculations indicate that carbene species F shows the nature of Fischer-type complexes, carbene species I reveals the character of Schrock-type carbene complexes, and carbene species C has the nature of both Fischer and Schrock types. Our computational results are in good agreement with the experiments. This study may help to design and develop more efficient catalysts for metal-mediated cyclopropanation reactions.

## ■ ASSOCIATED CONTENT

## ■ Supporting Information

Catalytic reaction pathway with the metallacyclobutane intermediate  $J'$  (path  $d'$ , Figure S1), natural bond orbitals for C, F, and I species (Figure S2), comparisons of DFT methods (Table S1), and tables and xyz files giving reaction coordinates for key transition states. This material is available free of charge via the Internet at <http://pubs.acs.org>.

## ■ AUTHOR INFORMATION

## Corresponding Authors

\*Y.-L.Z.: tel/fax, +86-21-34207190; e-mail, [yileizhao@sjtu.edu.cn](mailto:yileizhao@sjtu.edu.cn).

\*J.Z.: tel, +86-21-63846590-776922; fax, +86-21-64154900; e-mail, [jian.zhang@sjtu.edu.cn](mailto:jian.zhang@sjtu.edu.cn).

## Author Contributions

<sup>§</sup>These authors contributed equally to this work.

## Notes

The authors declare no competing financial interest.

## ■ ACKNOWLEDGMENTS

We thank the National Basic Research Program of China “973” (2013CB966800, 2012CB72100, 2010CB912702) and the National High-tech R&D Program of China “863” (2012AA020403), the National Natural Science Foundation of China (21102090, 20702031, 91230105, and 21377085), the Shanghai Municipal Education Commission (13YZ032), the Program for New Century Excellent Talents in University (NCET-12-0354 and NCET-12-0355), the Program for Professor of Special Appointment (Eastern Scholar) at Shanghai Institutions of Higher Learning, and the Shanghai Pujiang Program (10PJ406800 and 10PJ1405200) for financial support of this work. We thank Prof. Hualiang Jiang at the Shanghai Institute of Materia Medica (CAS, Shanghai, People's Republic of China), Dr. Lin Ling and Prof. Yixue Li at the Shanghai Institute of Organic Chemistry (CAS, Shanghai, People's Republic of China), and Prof. Huanwang Jing at Lanzhou University (Lanzhou, People's Republic of China) for comments and suggestions, and the SJTU-HPC computing facility award.

## ■ REFERENCES

- (1) (a) Yonezawa, S.; Yamamoto, T.; Yamakawa, H.; Muto, C.; Hosono, M.; Hattori, K.; Higashino, K.; Yutsudo, T.; Iwamoto, H.; Kondo, Y.; Sakagami, M.; Togame, H.; Tanaka, Y.; Nakano, T.; Takemoto, H.; Arisawa, M.; Shuto, S. *J. Med. Chem.* **2012**, *55*, 8838–8858. (b) Nguyen, X. C.; Longeon, A.; Pham, V. C.; Urvois, F.; Bressy, C.; Trinh, T. T. V.; Nguyen, H. N.; Phan, V. K.; Chau, V. M.; Briand, J.; Bourguet-Kondracki, M. *J. Nat. Prod.* **2013**, *76*, 1313–1318. (c) Suárez-Ortiz, G. A.; Cerda-García-Rojas, C. M.; Hernández-Rojas, A.; Pereda-Miranda, R. *J. Nat. Prod.* **2013**, *76*, 72–78.
- (2) (a) Kulinkovich, O. G. *Chem. Rev.* **2003**, *103*, 2597–2632. (b) Reissig, H. U.; Zimmer, R. *Chem. Rev.* **2003**, *103*, 1151–1196. (c) Pellissier, H. *Tetrahedron* **2010**, *66*, 8341–8375. (d) Hudlicky, T.; Reed, J. W. *Angew. Chem., Int. Ed.* **2010**, *49*, 4864–4876. (e) Mack, D. J.; Njardarson, J. T. *ACS Catal.* **2013**, *3*, 272–286.
- (3) (a) Kulinkovich, O. G.; de Meijere, A. *Chem. Rev.* **2000**, *100*, 2789–2834. (b) Lebel, H.; Marcoux, J. F.; Molinaro, C.; Charette, A. B. *Chem. Rev.* **2003**, *103*, 977–1050. (c) Pellissier, H. *Tetrahedron* **2008**, *64*, 7041–7095. (d) Kim, H. Y.; Salvi, L.; Carroll, P. J.; Walsh, P. J. *J. Am. Chem. Soc.* **2010**, *132*, 402–412.
- (4) Nozaki, H.; Moriuti, S.; Takaya, H.; Noyori, R. *Tetrahedron Lett.* **1966**, *7*, 5239–5244.
- (5) (a) Nishiyama, H.; Itoh, Y.; Matsumoto, H.; Park, S. B.; Itoh, K. *J. Am. Chem. Soc.* **1994**, *116*, 2223–2224. (b) Nishiyama, H.; Soeda, N.; Naito, T.; Motoyama, Y. *Tetrahedron: Asymmetry* **1998**, *9*, 2865–2869. (c) Motoyama, Y.; Kurihara, O.; Murata, K.; Aoki, K.; Nishiyama, H. *Organometallics* **2000**, *19*, 1025–1034.
- (6) (a) Huang, L.; Chen, Y.; Gao, G. Y.; Zhang, X. P. *J. Org. Chem.* **2003**, *68*, 8179–8184. (b) Chen, Y.; Fields, K. B.; Zhang, X. P. *J. Am. Chem. Soc.* **2004**, *126*, 14718–14719. (c) Chen, Y.; Ruppel, J. V.; Zhang, X. P. *J. Am. Chem. Soc.* **2007**, *129*, 12074–12075. (d) Zhu, S.; Ruppel, J. V.; Lu, H.; Wojtas, L.; Zhang, X. P. *J. Am. Chem. Soc.* **2008**, *130*, 5042–5043. (e) Ruppel, J. V.; Gauthier, T. J.; Snyder, N. L.; Perman, J. A.; Zhang, X. P. *Org. Lett.* **2009**, *11*, 2273–2276. (f) Doyle, M. P. *Angew. Chem., Int. Ed.* **2009**, *48*, 850–852. (g) Dzik, W. I.; Xu, X.; Zhang, X. P.; Reek, J. H.; Bruin, B. *J. Am. Chem. Soc.* **2010**, *132*, 10891–10902. (h) Zhu, S.; Xu, X.; Perman, J. A.; Zhang, X. P. *J. Am. Chem. Soc.* **2010**, *132*, 12796–12799.
- (7) Che, C. M.; Huang, J. S.; Lee, F. W.; Li, Y.; Lai, T. S.; Kwong, H. L.; Teng, P. F.; Lee, W. S.; Lo, W. C.; Peng, S. M.; Zhou, Z. Y. *J. Am. Chem. Soc.* **2001**, *123*, 4119–4129.
- (8) (a) Munslow, I. J.; Gillespie, K. M.; Deeth, R. J.; Scott, P. *Chem. Commun.* **2001**, *17*, 1638–1639. (b) Miller, J. A.; Gross, B. A.; Zhuravel, M. A.; Jin, W.; Nguyen, S. T. *Angew. Chem.* **2005**, *117*, 3953–3957. (c) Li, G. Y.; Zhang, J.; Chan, P. W. H.; Xu, Z. J.; Zhu, N. Y.; Che, C. M. *Organometallics* **2006**, *25*, 1676–1688. (d) Kanchiku, S.; Suematsu, H.; Matsumoto, K.; Uchida, T.; Katsuki, T. *Angew. Chem., Int. Ed.* **2007**, *46*, 3889–3891. (e) Xu, Z. J.; Fang, R.; Zhao, C. Y.; Huang, J. S.; Li, G. Y.; Zhu, N. Y.; Che, C. M. *J. Am. Chem. Soc.* **2009**, *131*, 4405–4417.
- (9) (a) Nakata, K.; Takeda, T.; Mihara, J.; Hamada, T.; Irie, R.; Katsuki, T. *Chem. Eur. J.* **2001**, *7*, 3776–3782. (b) Cussó, O.; Garcia-Bosch, I.; Ribas, X.; Lloret-Fillol, J.; Costas, M. *J. Am. Chem. Soc.* **2013**, *135*, 14871–14878. (c) Garcia-Bosch, I.; Gómez, L.; Polo, A.; Ribas, X.; Costas, M. *Adv. Synth. Catal.* **2012**, *354*, 65–70. (d) Garcia-Bosch, I.; Company, A.; Fontrodona, X.; Ribas, X.; Costas, M. *Org. Lett.* **2008**, *10*, 2095–2098. (e) Luts, T.; Frank, R.; Suprun, W.; Fritzsche, S.; Hey-Hawkins, E.; Papp, H. *J. Mol. Catal. A: Chem.* **2007**, *273*, 250–258.
- (10) (a) Kawabata, H.; Omura, K.; Katsuki, T. *Tetrahedron Lett.* **2006**, *47*, 1571–1574. (b) Kawabata, H.; Omura, K.; Uchida, T.; Katsuki, T. *Chem. Asian. J.* **2007**, *2*, 248–256. (c) Egloff, J.; Ranocchiari, M.; Schira, A.; Schotes, C.; Mezzetti, A. *Organometallics* **2013**, *32*, 4690–4701.
- (11) (a) Uchida, T.; Tamura, Y.; Ohba, M.; Katsuki, T. *Tetrahedron Lett.* **2003**, *44*, 7965–7968. (b) Tamura, Y.; Uchida, T.; Katsuki, T. *Tetrahedron Lett.* **2003**, *44*, 3301–3303. (c) Zhu, C.; Chen, X.; Yang, Z.; Du, X.; Liu, Y.; Cui, Y. *Chem. Commun.* **2013**, *49*, 7120–7122.
- (12) (a) Chow, C. P.; Shea, K. J. *J. Am. Chem. Soc.* **2005**, *127*, 3678–3679. (b) Wakabayashi, R.; Kurahashi, T.; Matsubara, S. *Org. Lett.* **2012**, *14*, 4794–4797.
- (13) (a) Reed, S. A.; White, M. C. *J. Am. Chem. Soc.* **2008**, *130*, 3316–3318. (b) Aguila, M. J. B.; Badiei, Y. M.; Warren, T. H. *J. Am. Chem. Soc.* **2013**, *135*, 9399–9406. (c) Ryu, J.; Kwak, J.; Shin, K.; Lee, D.; Chang, S. *J. Am. Chem. Soc.* **2013**, *135*, 12861–12868.
- (14) (a) Takatani, T.; Sears, J. S.; Sherrill, C. D. *J. Phys. Chem. A* **2009**, *113*, 9231–9236. (b) Takatani, T.; Sears, J. S.; Sherrill, C. D. *J. Phys. Chem. A* **2010**, *114*, 11714–11718.
- (15) (a) Kohn, W.; Sham, L. J. *Phys. Rev.* **1965**, *140*, 1133–1138. (b) Hohenberg, P.; Kohn, W. *Phys. Rev. B* **1964**, *136*, 864–871.
- (16) (a) Ikeno, T.; Iwakura, I.; Yabushita, S.; Yamada, T. *Org. Lett.* **2002**, *4*, 517–520. (b) Iwakura, I.; Ikeno, T.; Yamada, T. *Org. Lett.* **2004**, *6*, 949–952.
- (17) (a) Miller, J. A.; Jin, W.; Nguyen, S. T. *Angew. Chem., Int. Ed.* **2002**, *41*, 2953–2956. (b) Miller, J. A.; Gross, B. A.; Zhuravel, M. A.; Jin, W.; Nguyen, S. T. *Angew. Chem.* **2005**, *117*, 3953–3957.
- (18) (a) Foster, J.; Weinhold, F. *J. Am. Chem. Soc.* **1980**, *102*, 7211–7218. (b) Reed, A.; Weinhold, F. *J. Chem. Phys.* **1983**, *78*, 4066–4073. (c) Reed, A. E.; Weinstock, R. B.; Weinhold, F. *J. Chem. Phys.* **1985**, *83*, 735–746. (d) Reed, A. E.; Weinhold, F. *J. Chem. Phys.* **1985**, *83*, 1736–1740. (e) Reed, A. E.; Curtiss, L. A.; Weinhold, F. *Chem. Rev.* **1988**, *88*, 899–926. (f) Glendening, E. D.; Badenhoop, J. K.;

Reed, A. E.; Carpenter, J. E.; Bohmann, J. A.; Morales, C. M.; Weinhold, F. *Natural Bond Orbital Analysis*; 2001.

(19) (a) Tomasi, J.; Mennucci, B.; Cancès, E. *J. Mol. Struct. (THEOCHEM)* **1999**, *464*, 211–226. (b) Cossi, M.; Scalmani, G.; Rega, N.; Barone, V. *J. Chem. Phys.* **2002**, *117*, 43–54.

(20) Frisch, M. J.; Trucks, G. W.; Schlegel, H. B.; Scuseria, G. E.; Robb, M. A.; Cheeseman, J. R.; Scalmani, G.; Barone, V.; Mennucci, B.; Petersson, G. A.; Nakatsuji, H.; Caricato, M.; Li, X.; Hratchian, H. P.; Izmaylov, A. F.; Bloino, J.; Zheng, G.; Sonnenberg, J. L.; Hada, M.; Ehara, M.; Toyota, K.; Fukuda, R.; Hasegawa, J.; Ishida, M.; Nakajima, T.; Honda, Y.; Kitao, O.; Nakai, H.; Vreven, T.; Montgomery, J. A., Jr.; Peralta, J. E.; Ogliaro, F.; Bearpark, M.; Heyd, J. J.; Brothers, E.; Kudin, K. N.; Staroverov, V. N.; Kobayashi, R.; Normand, J.; Raghavachari, K.; Rendell, A.; Burant, J. C.; Iyengar, S. S.; Tomasi, J.; Cossi, M.; Rega, N.; Millam, J. M.; Klene, M.; Knox, J. E.; Cross, J. B.; Bakken, V.; Adamo, C.; Jaramillo, J.; Gomperts, R.; Stratmann, R. E.; Yazyev, O.; Austin, A. J.; Cammi, R.; Pomelli, C.; Ochterski, J. W.; Martin, R. L.; Morokuma, K.; Zakrzewski, V. G.; Voth, G. A.; Salvador, P.; Dannenberg, J. J.; Dapprich, S.; Daniels, A. D.; Farkas, Ö.; Foresman, J. B.; Ortiz, J. V.; Cioslowski, J.; Fox, D. J. *Gaussian 09*; Gaussian, Inc., Wallingford, CT, 2009.

(21) (a) Becke, A. D. *J. Chem. Phys.* **1993**, *98*, 1372–1377. (b) Becke, A. D. *J. Chem. Phys.* **1993**, *98*, 5648–5652. (c) Lee, C.; Yang, W.; Parr, R. G. *Phys. Rev. B* **1988**, *37*, 785–789.

(22) (a) Petersson, G. A.; Bennett, A.; Tensfeldt, T. G.; Al-Laham, M. A.; Shirley, W. A.; Mantzaris, J. *J. Chem. Phys.* **1988**, *89*, 2193–2218. (b) Petersson, G. A.; Al-Laham, M. A. *J. Chem. Phys.* **1991**, *94*, 6081–6090. (c) Rassolov, V. A.; Pople, J. A.; Ratner, M. A.; Windus, T. L. *J. Chem. Phys.* **1998**, *109*, 1223–1229. (d) Rassolov, V. A.; Ratner, M. A.; Pople, J. A.; Redfern, P. C.; Curtiss, L. A. *J. Comput. Chem.* **2001**, *22*, 976–984.

(23) (a) Hay, P. J.; Wadt, W. R. *J. Chem. Phys.* **1985**, *82*, 270–283. (b) Wadt, W. R.; Hay, P. J. *J. Chem. Phys.* **1985**, *82*, 284–298. 284–98. (c) Hay, P. J.; Wadt, W. R. *J. Chem. Phys.* **1985**, *82*, 299–310. (d) Dunning, T. H., Jr. *J. Chem. Phys.* **1989**, *90*, 1007–1023.

(24) (a) McLean, D.; Chandler, G. S. *J. Chem. Phys.* **1980**, *72*, 5639–5648. (b) Raghavachari, K.; Binkley, J. S.; Seeger, R.; Pople, J. A. *J. Chem. Phys.* **1980**, *72*, 650–654.

(25) Marenich, A. V.; Cramer, C. J.; Truhlar, D. G. *J. Phys. Chem. B* **2009**, *113*, 6378–6396.

(26) Zhao, Y.; Truhlar, D. G. *Theor. Chem. Acc.* **2008**, *120*, 215–241.

(27) (a) Perdew, J. P.; Burke, K.; Ernzerhof, M. *Phys. Rev. Lett.* **1996**, *77*, 3865–3868. (b) Perdew, J. P.; Burke, K.; Ernzerhof, M. *Phys. Rev. Lett.* **1997**, *78*, 1396–1396. (c) Adamo, C.; Barone, V. *J. Chem. Phys.* **1999**, *110*, 6158–6169.

(28) Hamaker, C. G.; Djukic, J.-P.; Smith, D. A.; Woo, L. K. *Organometallics* **2001**, *20*, 5189–5199.

(29) Fischer, H.; Radom, L. *Angew. Chem., Int. Ed.* **2001**, *40*, 1340–1371.

(30) Fischer, E. O.; Maasbol, A. *Angew. Chem., Int. Ed.* **1964**, *3*, 580–581.

(31) Schrock, R. R. *J. Am. Chem. Soc.* **1974**, *96*, 6796–6797.